

Space Charge Transfer in Hybrid Inorganic/Organic Systems

Yong Xu^{1,*}, Oliver T. Hofmann¹, Raphael Schlesinger², Stefanie Winkler³,
Johannes Frisch², Jens Niederhausen², Antje Vollmer³, Sylke Blumstengel²,
Fritz Henneberger², Norbert Koch^{2,3}, Patrick Rinke¹, and Matthias Scheffler¹

¹*Fritz-Haber-Institut der Max-Planck-Gesellschaft, 14195 Berlin, Germany*

²*Humboldt-Universität zu Berlin, Institut für Physik, 12489 Berlin, Germany*

³*Helmholtz-Zentrum Berlin für Materialien und
Energie GmbH-BESSY II, 12489 Berlin, Germany*

Abstract

We discuss density functional theory calculations of hybrid inorganic/organic systems (HIOS) that explicitly include the global effects of doping (i.e. position of the Fermi level) and the formation of a space-charge layer. For the example of tetrafluoro-tetracyanoquinodimethane (F4TCNQ) on the ZnO(000 $\bar{1}$) surface we show that the adsorption energy and electron transfer depend strongly on the ZnO doping. The associated work function changes are large, for which the formation of space-charge layers is the main driving force. The prominent doping effects are expected to be quite general for charge-transfer interfaces in HIOS and important for device design.

PACS numbers: 68.43.-h, 71.15.-m, 71.15.Mb, 73.20.-r

Hybrid inorganic/organic systems (HIOS) have already been applied in (opto)electronics, including solar cells [1], laser diodes [2], light emitting diodes [3] or sensors [4]. Recently HIOS have attracted enormous research interest owing to their promise to synergetically combine the best features of two worlds. This could be, for example, the high charge carrier mobility and efficient charge injection of inorganic semiconductors, and the strong light-matter coupling and large chemical compound space of organic semiconductors.

In HIOS research, first-principles approaches are indispensable due to the atomistic insight they provide. These calculations do typically not include the global effects of doping (i.e. the position of the electron chemical potential or Fermi level that is controlled by doping). However, if donor or acceptor states are present at the interface of HIOS, the Fermi level position significantly affects the energy-level alignment (cf Fig. 1), as we will demonstrate with quantitative electronic-structure calculations in this Letter. A crucial aspect is the formation of a space-charge layer at surfaces and interfaces that gives rise to band bending. Since semiconductors are always intentionally or unintentionally doped, it is paramount to include doping explicitly in the theoretical description – both the global effects as well as the formation of space-charge layers.

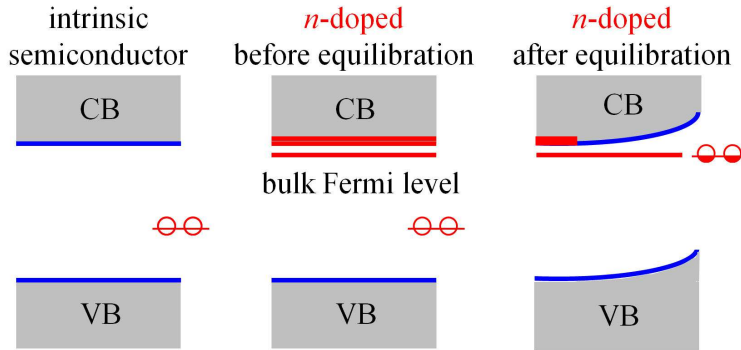


FIG. 1. (color online) Schematic illustration of the electron transfer to acceptor states at a surface or interface of a n -doped semiconductor (middle and right). In an undoped intrinsic semiconductor (left) no such electron transfer can take place resulting in an empty acceptor state in the band gap.

To illustrate doping effects in HIOS, we consider the general problem of (organic) adsorbates on doped (inorganic) semiconductors, and investigate the properties of adsorbates as a function of the substrate doping concentration. We here adopt an approach for the calculation of defects in semiconductors [5–7], which combines the statistical concept of a bulk Fermi level with atomistic first-principles calculations. In addition, we show how

a space-charge layer, whose macroscopic dimensions far exceed the dimensions of super-cells tractable in standard density-functional theory (DFT) calculations, can be properly accounted for. Then we apply the approach to DFT calculations of an example HIOS: a tetrafluoro-tetracyanoquinodimethane (F4TCNQ) monolayer on the ZnO(000 $\bar{1}$) (2 \times 1)-H surface (see Fig. 2). We show that the doping in HIOS quantitatively affects interface properties such as the adsorption energy and electron transfer, or even qualitatively change the energy-level alignment at the interface. On *n*-doped ZnO, F4TCNQ induces a large work function increase. This is accompanied by electron transfer that becomes vanishingly small in the limit of low bulk doping concentrations. Such a behavior has recently been demonstrated in photoemission measurements for F4TCNQ on ZnO [8].

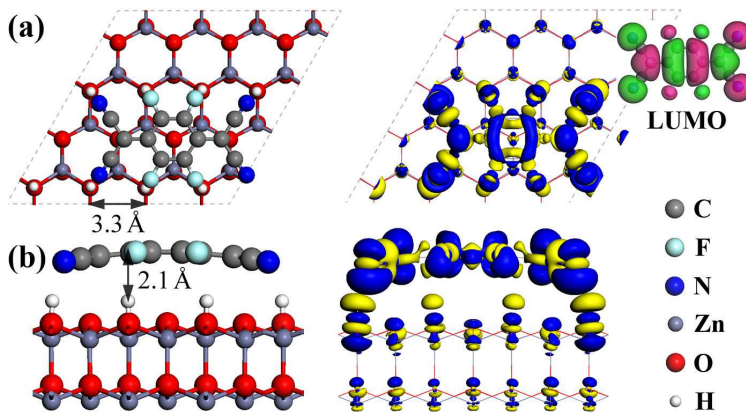


FIG. 2. (color online) Geometry of F4TCNQ adsorbed on ZnO(000 $\bar{1}$) (2 \times 1)-H (left) and the adsorption-induced electron density rearrangement for *n*-doped ZnO (right): (a) top view and (b) side view (upper part only). Electrons flow from the yellow to blue areas upon adsorption. On the molecular side, the region that gains electrons upon adsorption mimics the shape of the lowest unoccupied molecular orbital (LUMO) of the free F4TCNQ molecule (depicted in the upper right).

A computational approach to describe doping effects for (organic) adsorbates on doped (inorganic) semiconductors should include (i) a Fermi level that depends on the bulk dopant concentration N_D , (ii) electrons or holes that can be exchanged with the adsorbate, and (iii) the ensuing space-charge layer that leads to band bending. In the following we demonstrate how to incorporate these three factors into a DFT-based framework.

Analogous to calculations of defects in the bulk or at interfaces [5–7], excess electrons or holes are introduced into the semiconductor to model the global effects of doping. The adsorption energy (ΔE_q^{ads}) of an adsorbate that receives q electrons from the electron reservoir

with an electron chemical potential ϵ_F can be written as [9]

$$\Delta E_q^{\text{ads}}(\epsilon_F) = (-E_q^{\text{surf/mol}} + E_q^{\text{surf}} + E_0^{\text{mol}}) + (q\Delta\epsilon_F - q\delta) + \Delta E^{\text{SC}}. \quad (1)$$

$E_q^{\text{surf/mol}}$ and E_q^{surf} are the total energies of the adsorbate system and the bare substrate computed in a supercell with q excess electrons, and E_0^{mol} is the total energy of the neutral molecule. The second term in Eq. (1) quantifies the energy of the excess charge with respect to the electron reservoir: $\Delta\epsilon_F = \epsilon_F - \epsilon_{\text{CBm}}$ when charging electrons ($q > 0$) and $\Delta\epsilon_F = \epsilon_F - \epsilon_{\text{VBM}}$ for holes ($q < 0$), where ϵ_{CBm} is the conduction band minimum (CBm) and ϵ_{VBM} is the valence band maximum (VBM). Since the excess charge can fill the substrate's conduction (or valence) bands to an average energy δ , $q\delta$ is a finite-filling correction. δ depends on q and reduces to zero in the limit of small q [9]. In our calculations it never exceeds 0.2 eV. The last term in Eq. (1), ΔE^{SC} , denotes the energy correction for describing the space-charge layer.

Introducing excess charges into the unit cell is common practice in first-principles calculations of defects in the bulk [5–7, 10–13]. To keep the unit cell overall charge neutral and therefore to avoid a diverging Hartree energy, a uniform, compensating background of opposite charge is introduced. However, for surface calculations in the periodic slab approach a homogeneous compensating background cannot be used. The reason is that the background charge also resides in the vacuum region between the repeated slabs, and therefore builds up a dipole with the original charge that is confined to the slab. This dipole and the associated energy diverge for increasing vacuum separations. To circumvent this problem we confine the compensating charge by applying the virtual-crystal approximation (VCA) [14–16]. We modify the nuclear charge of semiconductor substrate atoms by a small amount ΔZ [15–17], which results in corresponding excess electrons or holes in either the conduction or valence band. Independent tests show that in the limit of small ΔZ the VCA method provides a very reliable description of doping effects at surfaces [16].

An important feature of semiconductor surfaces is that charge transfer from bulk dopants generates a space-charge layer and induces band bending. While a direct description of space-charge layers in first-principles calculations is computationally formidable because of the large length scales involved (~ 100 nm for ZnO with $N_D = 10^{17} \text{ cm}^{-3}$), the effect can be taken into account using simple electrostatic considerations. For macroscopically extended (potentially semi-infinite) semiconductor surfaces, this electrostatic description is textbook

knowledge [18]. The transfer of q electrons (per surface supercell area A) from bulk dopants to the surface costs an energy of

$$E_1^{\text{SC}}(q, N_{\text{D}}) = \frac{e^2}{6\varepsilon\varepsilon_0 N_{\text{D}} A^2} |q|^3, \quad (2)$$

where e is the elementary charge, ε the static dielectric constant and ε_0 the vacuum permittivity [18].

Care has to be taken, however, because the DFT slab calculations also include a certain amount of band bending. The spatial extend of the space-charge layer is limited by the thickness of the slab (d) in the atomistic model. The concentration of excess charge in the supercell is then $N'_{\text{D}} = |q|/(Ad)$. To estimate the electrostatic energy of forming a space-charge layer within the slab, we apply Eq. (2) and replace N_{D} by N'_{D} :

$$E_2^{\text{SC}}(q) = \frac{e^2 d}{6\varepsilon\varepsilon_0 A} q^2. \quad (3)$$

We then take $\Delta E^{\text{SC}} = -E_1^{\text{SC}}(q, N_{\text{D}}) + E_2^{\text{SC}}(q)$ as the space-charge layer correction to the adsorption energy. Equations (2) and (3) demonstrate clearly that the electrostatic energy of a space-charge layer in a realistic semiconductor differs from that in the DFT slab calculations by its q -dependence. However, with the exception of Ref. 16 no such correction term has been taken into account in electronic-structure studies so far. As we will demonstrate, the correction affects the predicted electron transfer and adsorption energy considerably, and thus is essential in DFT studies of HIOS. Since the inclusion of ΔE^{SC} permits us to decouple N_{D} from the excess electrons or holes introduced in the supercell, we rewrite the adsorption energy as a function of N_{D} :

$$\begin{aligned} \Delta E_q^{\text{ads}}(N_{\text{D}}) = & (-E_q^{\text{surf/mol}} + E_q^{\text{surf}} + E_0^{\text{mol}}) + [q\Delta\epsilon_{\text{F}}(N_{\text{D}}) - q\delta] \\ & - \frac{e^2}{6\varepsilon\varepsilon_0 N_{\text{D}} A^2} |q|^3 + \frac{e^2 d}{6\varepsilon\varepsilon_0 A} q^2. \end{aligned} \quad (4)$$

The N_{D} dependence of the Fermi level $[\Delta\epsilon_{\text{F}}(N_{\text{D}})]$ is known for many semiconductors and is described in the Supplemental Material [9] for ZnO.

Next, we apply our approach to a F4TCNQ monolayer on the ZnO(000 $\bar{1}$) surface (shown in Fig. 2). F4TCNQ is a strong electron acceptor, that is commonly used for surface/interface modifications and work function tuning [8, 19–22]. ZnO is a suitable inorganic component in HIOS, and is natively n -doped, presumably due to defects like oxygen vacancies, zinc

interstitials or hydrogen [23–25]. The oxygen-terminated ZnO(000 $\bar{1}$) surface has been extensively studied [26–28]. The ZnO(000 $\bar{1}$) (2 \times 1)-H phase, in which every second row of surface O atoms is decorated with H atoms, is the thermodynamically most stable structure at typical experimental growth conditions, according to our and previous studies [17, 27, 28]. We also showed previously that ZnO(000 $\bar{1}$) surfaces with lower hydrogen concentrations (less than 50%) may be stabilized by *n*-type bulk dopants in hydrogen-deficient environments [17]. However, this does not affect our conclusions. For simplicity, we assume hydrogen-rich environments and adopt the ZnO(000 $\bar{1}$) (2 \times 1)-H surface as model for the bare surface prior to F4TCNQ adsorption.

The DFT calculations were performed using the all-electron full-potential code FHI-aims [29]. The ZnO surface was modeled by a four double-layer slab with the top two layers relaxed and the bottom end saturated by H atoms of charge 1.5 *e* at a relaxed geometry. The periodic slab approach was employed with a 50 Å vacuum separation and dipole corrections between periodic images [30, 31]. Increasing the slab thickness affects the calculated adsorption energies by only a few meV. To introduce excess electrons or holes, we modified the nuclear charges of Zn and O by a small amount $\Delta Z = q/N$ in the VCA method [14, 15], where *N* is the total number of Zn and O atoms. Here *N* = 128 and ΔZ is 0.01 at most. The slab calculations were performed with a 4 \times 4 \times 1 Γ -centered k-grid and a Gaussian broadening of 0.1 eV. We applied the Heyd-Scuseria-Ernzerhof (HSE) hybrid functional [32, 33], but the admixture of exact-exchange was adjusted to 50% (this functional is denoted HSE*, in the following) as in Ref. 34, instead of the default value of 25% to achieve the best compromise between the experimental bandwidth, the band gap and the energetic ordering for the two subsystems. With 4.3 eV the band gap of ZnO is then overestimated compared to the experimental value of 3.44 eV at zero temperature [35]. Equilibrium geometries were calculated with the Perdew-Burke-Ernzerhof (PBE) functional [36] combined with screened van der Waals (vdW) corrections [37] (PBE+vdW^{scr}) excluding vdW interactions within the ZnO substrate. Tests for HSE*+vdW^{scr} show negligible geometry differences. We used the following vdW parameters (*C*₆, α , *R*⁰) for Zn (54.978, 15.055, 2.903) and O (4.644, 4.377, 2.974). The electronic structure and adsorption energies were calculated using HSE*+vdW^{scr}.

On the ZnO(000 $\bar{1}$) (2 \times 1)-H surface, the four CN groups of F4TCNQ interact attractively with the surface H atoms and repulsively with the surface O atoms. This results in a stable geometry (see Fig. 2), in which F4TCNQ lies face-on on the substrate with the cyano groups

located above the surface H atoms. The molecule distorts slightly upon adsorption, placing the N atoms 0.4 Å below the F atoms. We also found some metastable geometries at other adsorption sites, whose energies are at least 0.5 eV higher. The monolayer morphology depends on the molecular coverage. At low coverages, the F4TCNQ molecules tend to be well separated from each other due to intermolecular repulsions, even in the limit of zero electron transfer. At high coverages, the intermolecular repulsion has a more direct influence on the packing motif. Here we focus on the coverage of 0.67 molecule/nm², which is the tightest monolayer packing that is commensurate with the H-overlayer and was used to study F4TCNQ on coinage metals [20, 21]. Figure 2 shows the most stable monolayer structure we found. Doping has a negligible influence on the adsorption geometry for the given molecular coverage and substrate structure. According to our tests, the molecule-substrate distance decreases by less than 0.05 Å when ZnO becomes *n*-doped. The bond distance thus depends much weaker on the adsorption induced charge transfer than for organic molecules on metal substrates [38], a point that has to be revisited in the future. Slight variations in the packing motif (e.g. relative molecular displacements or rotations) result in structures with similar energy, but the same electronic structure. From this we conclude that the monolayer most likely consists of a disordered arrangement of flat-lying molecules, whose electronic structure is a superposition of molecular electronic structures. For a given coverage the alternative geometries therefore result in the same amount of electron transfer and work function change.

Figure 3 summarizes our results based on Eq. 1, but without the space-charge correction. For undoped calculations the LUMO' (LUMO after adsorption) of F4TCNQ lies in the band gap and is unoccupied [see Fig. 3(a)]. As soon as excess electrons are offered (i.e. $q > 0$), these are immediately transferred to the LUMO' of F4TCNQ [see Fig. 3(b)], which is further evidenced by the adsorption induced charge rearrangement (see Fig. 2). As a result the work function increases. Due to the linear term $q\Delta\epsilon_F$ in Eq. 1, calculations for different q manifest themselves in lines with different slopes in Fig. 3. For a given Fermi energy, the line with the lowest energy indicates how much charge is transferred to F4TCNQ. Figure 3 illustrates that the adsorption energy depends quadratically on the Fermi energy. Such a quadratic behavior is expected from a simplified parallel capacitor model for the charge transfer between the substrate and the adsorbate. The DFT results therefore show that i) the electron transfer and adsorption energy increase with increasing Fermi level and that ii) undoped calculations (i.e. the majority of all surface calculations in the literature) do not capture this effect and

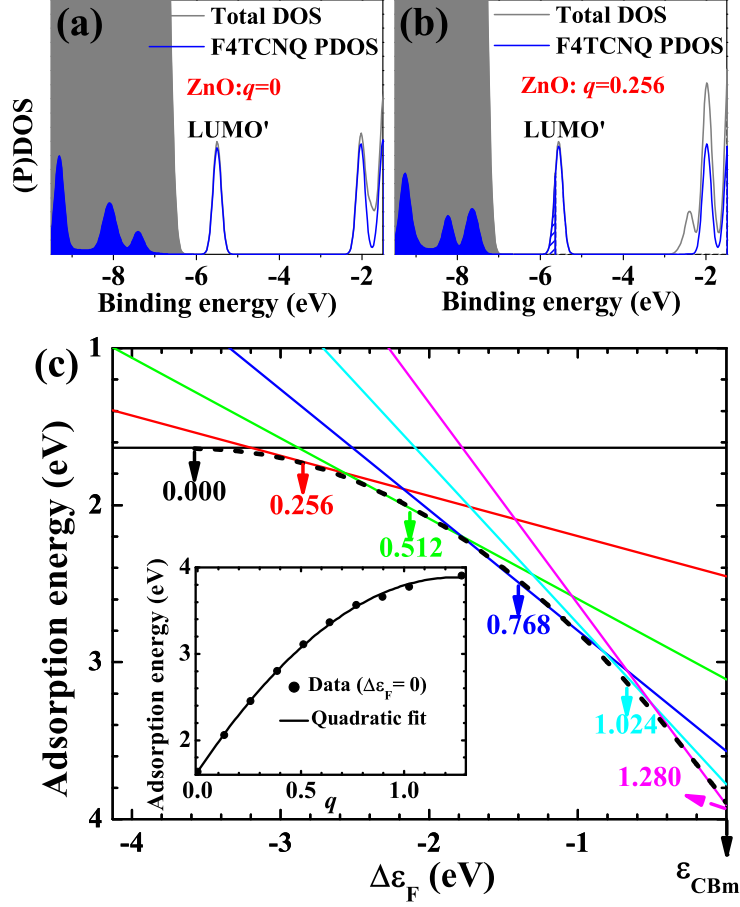


FIG. 3. (color online) (a,b) The calculated total density of states (DOS) and projected DOS (PDOS) onto F4TCNQ for intrinsic ($q = 0$) and electron-doped ($q = 0.256$) ZnO, where $\Delta Z = q/128$. The position at which the LUMO' pins in (b) corresponds to the Fermi level at the surface, which is determined by the space-charge layer. The binding energy is referenced to the vacuum level. (c) Adsorption energy as a function of $\Delta\epsilon_F = \epsilon_F - \epsilon_{CBm}$ for different charge states q (indicated by the corresponding numbers), obtained by Eq. (1) excluding ΔE^{SC} . The inset shows data points of the adsorption energy versus q at $\Delta\epsilon_F = 0$ and a quadratic fit. The fit then gives the adsorption energy as a function of $\Delta\epsilon_F$ (dashed line in the main figure), which also exhibits a quadratic dependence.

predict zero electron transfer and vacuum level alignment (cf Fig. 1).

If the Fermi level position at the surface is known experimentally, the amount of electron transfer and the corresponding adsorption energy can be read off Fig. 3, once the data has been corrected for the erroneous space-charge layer present in the slab calculations. To

proceed, we include the space-charge layer correction using Eq. 4. For a given N_D , we maximize $\Delta E_q^{\text{ads}}(N_D)$ with respect to q , which then gives the optimal electron transfer per molecule Q and the associated adsorption energy ΔE^{ads} .

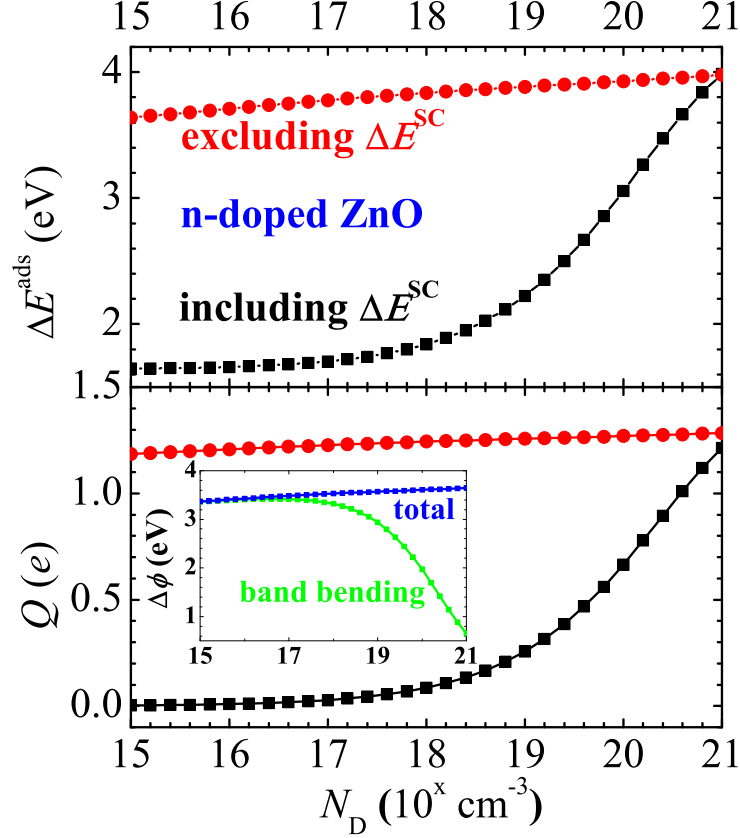


FIG. 4. (color online) Adsorption energy ΔE^{ads} and electron transfer Q as a function of (n -type) dopant concentration N_D for F4TCNQ/ZnO(000 $\bar{1}$) (2 \times 1)-H, calculated excluding and including the space-charge layer correction ΔE^{SC} . The F4TCNQ-induced work function change $\Delta\phi$ and the associated band-bending contribution (from calculations including ΔE^{SC}) are shown in the inset.

The result is shown in Fig. 4, which summarizes the main message of this Letter. Both the electron transfer and adsorption energy exhibit a pronounced dependence on N_D . It is well known that the magnitude of band bending is inversely proportional to N_D . Therefore, for low N_D band bending alone can lift up the LUMO' to the Fermi energy, inducing a large work function increase (inset of Fig. 4). This reduces the required electron transfer to nearly zero and the adsorption energy assumes the value of 1.6 eV we find in the undoped calculation. As N_D increases, the work functions before and after adsorption only slightly

vary, and the work function change depends weakly on N_D (inset of Fig. 4). While band bending reduces the electron transfer picks up. In the process, the adsorption energy more than doubles. For heavily n -doped ZnO used in transparent conductors, the adsorption energy has increased by more than 2 eV to a value of 4.0 eV. For comparison, without the space-charge layer correction the DFT results (red line in Fig. 4) miss the N_D dependence entirely and only give reasonable results in the high-doping region.

Real HIOS interfaces are typically not as “ideal” as the ones discussed here. Realistic models would have to include not only the spatial profile of the dopants, but also information on other impurities at or near the interface (e.g. oxygen vacancies [23]) that could pin the Fermi level at defect levels [39] and limit the amount of band bending. In some cases the ZnO films may be thinner than the space-charge layer or ZnO nanoclusters or nanocolumns are used. Then we expect doping effects to be film-thickness/structure-size dependent. All these issues could be important for HIOS, but their resolution requires input from experiments.

Finally, we make contact with recent photoemission experiments for F4TCNQ on ZnO(000 $\bar{1}$) [8]. We predict for n -doped ZnO that the work function increases up to around 5.7 eV upon adsorption, due to the partial occupation and pinning of the LUMO' at the Fermi level. This final work function is insensitive to variations in the surface termination (i.e. the hydrogen deficiency alluded to before), because it is determined by the distance of the LUMO' to the vacuum level above the F4TCNQ film and thus independent from the position of the LUMO' in the band gap. At the experimental N_D of approx. 10^{17} cm^{-3} , Fig. 4 predicts a vanishing electron transfer of 0.03 electrons/molecule (or 0.02 electrons/nm²). The results are consistent with the photoemission measurements, which observe a final work function of 5.9 eV and no noticeable electron transfer [8]. While band bending dominates the work function change in our theoretical description, band bending is limited to 0.5 eV in experiment [8], possibly because of a different interface structure and pinning at deep defect states.

It is in principle possible to change the level alignment at a HIOS interface from Fermi-level pinning to vacuum level alignment. For the example of F4TCNQ on ZnO(000 $\bar{1}$) (2 \times 1)-H, we demonstrate that such a transition occurs when the substrate doping varies from n to p -type. This behavior is expected to be quite general in HIOS and it would be interesting to experimentally test also materials like GaN or Si. Moreover, we show that the amount of electron transfer and therefore the amount of trapped charge at the interface significantly

depend on the bulk doping concentration. The trapped charges can act as scattering centers and affect transport properties at the interface. Therefore, high bulk doping concentrations for improved charge injection/transport have to be balanced against the resulting interface charges for device optimization.

This work is supported by the DFG collaborative research project 951 “HIOS”. Y. Xu acknowledges support from the Alexander von Humboldt foundation.

* yongxu@fhi-berlin.mpg.de

- [1] M. Law, L. Greene, J. Johnson, R. Saykally, and P. Yang, Nat. Mater. **4**, 455 (2005)
- [2] Y. Yang, G. Turnbull, and I. Samuel, Appl. Phys. Lett. **92**, 163306 (2008)
- [3] M. Sessolo and H. Bolink, Adv. Mater. **23**, 1829 (2011)
- [4] J. Levell, M. Giardini, and I. Samuel, Opt. Express **18**, 3219 (2010)
- [5] C. Weinert and M. Scheffler, Mat. Sci. Forum **10-12**, 25 (1986)
- [6] M. Scheffler and J. Dabrowski, Phil. Mag. A **58**, 107 (1988)
- [7] U. Scherz and M. Scheffler, in *Imperfections in III/V Materials*, Semiconductors and Semimetals, Vol. 38, edited by E. R. Weber (Academic, New York, 1993) p. 1
- [8] R. Schlesinger, Y. Xu, O. T. Hofmann, S. Winkler, J. Frisch, J. Niederhausen, A. Vollmer, S. Blumstengel, F. Henneberger, P. Rinke, M. Scheffler, and N. Koch, Phys. Rev. B **87**, 155311 (2013)
- [9] See Supplemental Material
- [10] C. G. Van de Walle, P. J. H. Denteneer, Y. Bar-Yam, and S. T. Pantelides, Phys. Rev. B **39**, 10791 (1989)
- [11] S. B. Zhang and J. E. Northrup, Phys. Rev. Lett. **67**, 2339 (1991)
- [12] C. G. Van de Walle and J. Neugebauer, J. Appl. Phys. **95**, 3851 (2004)
- [13] C. Persson, Y. J. Zhao, S. Lany, and A. Zunger, Phys. Rev. B **72**, 035211 (2005)
- [14] L. Vegard, Z. Phys. **5**, 17 (1921)
- [15] M. Scheffler, Physica B **146**, 176 (1987)
- [16] N. Richter, S. Siculo, S. Levchenko, J. Sauer, and M. Scheffler, arXiv:1305.5157 (accepted by Phys. Rev. Lett.).
- [17] N. Moll, Y. Xu, O. T. Hofmann, and P. Rinke, to be published

- [18] S. Sze and K. Ng, *Physics of semiconductor devices* (Wiley-interscience, 2006)
- [19] N. Koch, S. Duhm, J. P. Rabe, A. Vollmer, and R. L. Johnson, Phys. Rev. Lett. **95**, 237601 (2005)
- [20] L. Romaner, G. Heimel, J.-L. Bredas, A. Gerlach, F. Schreiber, R. L. Johnson, J. Zegenhagen, S. Duhm, N. Koch, and E. Zojer, Phys. Rev. Lett. **99**, 256801 (2007)
- [21] G. M. Rangger, O. T. Hofmann, L. Romaner, G. Heimel, B. Bröcker, R.-P. Blum, R. L. Johnson, N. Koch, and E. Zojer, Phys. Rev. B **79**, 165306 (2009)
- [22] W. Chen, D. Qi, X. Gao, and A. Wee, Prog. Surf. Sci. **84**, 279 (2009)
- [23] U. Ozgur, Y. I. Alivov, C. Liu, A. Teke, M. A. Reshchikov, S. Dogan, V. Avrutin, S.-J. Cho, and H. Morkoc, J. Appl. Phys. **98**, 041301 (2005)
- [24] C. G. Van de Walle, Phys. Rev. Lett. **85**, 1012 (2000)
- [25] A. Janotti and C. G. Van de Walle, Nature Mater. **6**, 44 (2006)
- [26] C. Wöll, Prog. Surf. Sci. **82**, 55 (2007)
- [27] B. Meyer, Phys. Rev. B **69**, 045416 (2004)
- [28] J. V. Lauritsen, S. Porsgaard, M. K. Rasmussen, M. C. R. Jensen, R. Bechstein, K. Meinander, B. S. Clausen, S. Helveg, R. Wahl, G. Kresse, and F. Besenbacher, ACS Nano **5**, 5987 (2011)
- [29] V. Blum, R. Gehrke, F. Hanke, P. Havu, V. Havu, X. Ren, K. Reuter, and M. Scheffler, Comp. Phys. Comm. **180**, 2175 (2009)
- [30] J. Neugebauer and M. Scheffler, Phys. Rev. B **46**, 16067 (1992)
- [31] L. Bengtsson, Phys. Rev. B **59**, 12301 (1999)
- [32] J. Heyd, G. E. Scuseria, and M. Ernzerhof, J. Chem. Phys. **118**, 8207 (2003)
- [33] A. V. Krukau, O. A. Vydrov, A. F. Izmaylov, and G. E. Scuseria, J. Chem. Phys. **125**, 224106 (2006)
- [34] R. Ramprasad, H. Zhu, P. Rinke, and M. Scheffler, Phys. Rev. Lett. **108**, 066404 (2012)
- [35] M. Cardona and M. L. W. Thewalt, Rev. Mod. Phys. **77**, 1173 (Nov 2005)
- [36] J. P. Perdew, K. Burke, and M. Ernzerhof, Phys. Rev. Lett. **77**, 3865 (1996)
- [37] G.-X. Zhang, A. Tkatchenko, J. Paier, H. Appel, and M. Scheffler, Phys. Rev. Lett. **107**, 245501 (2011)
- [38] S. Duhm, A. Gerlach, I. Salzmann, B. Bröcker, R. Johnson, F. Schreiber, and N. Koch, Organic Electronics **9**, 111 (2008)
- [39] H. Mosbacker, Y. Strzhemechny, B. White, P. Smith, D. C. Look, D. Reynolds, C. Litton,

and L. Brillson, Appl. Phys. Lett. **87**, 012102 (2005)